


Association Between Serotonin Denervation and Resting-State Functional Connectivity in Mild Cognitive Impairment

Frederick S. Barrett ^{1,*}, Clifford I. Workman,¹ Haris I. Sair,²
Alena V. Savonenko,³ Michael A. Kraut,² Devin J. Sodums,¹ Jin J. Joo,¹
Najlla Nassery,⁴ Christopher M. Marano,¹ Cynthia A. Munro,¹ Jason Brandt,¹
Yun Zhou,⁵ Dean F. Wong,⁵ and Gwenn S. Smith^{1,2}

¹Department of Psychiatry and Behavioral Sciences, Johns Hopkins University School of Medicine, Baltimore, Maryland

²Department of Radiology and Radiological Sciences, Division of Neuroradiology, Johns Hopkins University School of Medicine, Baltimore, Maryland

³Department of Pathology (Neuropathology), Johns Hopkins University School of Medicine, Baltimore, Maryland

⁴Division of General Internal Medicine, Johns Hopkins University School of Medicine, Baltimore, Maryland

⁵Department of Radiology and Radiological Sciences, Section of High Resolution Brain PET Imaging, Johns Hopkins University School of Medicine, Baltimore, Maryland

Abstract: Resting-state functional connectivity alterations have been demonstrated in Alzheimer's disease (AD) and mild cognitive impairment (MCI) before the observation of AD neuropathology, but mechanisms driving these changes are not well understood. Serotonin neurodegeneration has been observed in MCI and AD and is associated with cognitive deficits and neuropsychiatric symptoms, but the role of the serotonin system in relation to brain network dysfunction has not been a major focus of investigation. The current study investigated the relationship between serotonin transporter availability (SERT; measured using positron emission tomography) and brain network functional connectivity (measured using resting-state functional MRI) in 20 participants with MCI and 21 healthy controls. Two SERT regions of interest were selected for the analysis: the Dorsal Raphe Nuclei (DRN) and the precuneus which represent the cell bodies of origin and a cortical target of projections of the serotonin system, respectively. Both regions show decreased SERT in MCI compared to controls and are the site of early AD pathology. Average resting-state functional connectivity did not differ between MCI and controls. Decreased SERT in DRN was associated with lower hippocampal resting-state connectivity in MCI participants compared to controls. Decreased SERT in the right precuneus was also associated with lower resting-state connectivity of the retrosplenial cortex to the dorsal lateral prefrontal cortex and higher resting-state connectivity of the retrosplenial cortex to the posterior cingulate and in

Contract grant sponsor: National Institute of Health; Contract grant numbers: AG038893, AG041633, UL1 TR 001079, T32 DA007209 (to F.S.B.), and R03 DA042336 (to F.S.B.).

*Correspondence to: Frederick S. Barrett, Department of Psychiatry and Behavioral Sciences, Johns Hopkins University School of Medicine, 5510 Nathan Shock Dr., Baltimore, MD 21224. E-mail: fbarret2@jhu.edu

Received for publication 26 October 2016; Revised 14 March 2017; Accepted 20 March 2017.

DOI: 10.1002/hbm.23595

Published online 5 April 2017 in Wiley Online Library (wileyonlinelibrary.com).

patients with MCI but not in controls. These results suggest that a serotonergic mechanism may underlie changes in brain functional connectivity in MCI. *Hum Brain Mapp* 38:3391–3401, 2017. © 2017 Wiley Periodicals, Inc.

Key words: functional magnetic resonance imaging (fMRI); positron emission tomography (PET); serotonin transporter; resting state functional magnetic resonance imaging (rs-fMRI); individual differences

INTRODUCTION

Resting-state functional magnetic resonance imaging (rs-fMRI) can be used to derive correlations in time-varying blood-oxygenation level dependent (BOLD) signal collected when participants are at rest (e.g. resting-state functional connectivity). This method has been shown to identify consistent, replicable sets of brain regions that covary [Damoiseaux et al., 2006], which are referred to as networks. Resting-state functional connectivity networks reflect structural connectivity patterns [Damoiseaux et al., 2009; Greicius et al., 2009; van den Heuvel et al., 2009] and are thought to reflect the intrinsic organization of brain activity [Buckner et al., 2008; Fox and Raichle, 2007] and communication between distinct areas of the brain [van den Heuvel and Sporns, 2013; van den Heuvel et al., 2009]. The spatial organization of resting-state functional connectivity networks overlaps with well-known and empirically validated networks of brain areas that support basic psychological processes such as perception, attention, and internally directed thought [Fox and Raichle, 2007; Smith et al., 2009].

Alterations in resting-state functional connectivity in specific networks have been observed in normal aging [Agcaoglu et al., 2015; Damoiseaux et al., 2008; Ferreira and Busatto, 2013; Keller et al., 2015] and in patients with Alzheimer's dementia (AD) [Damoiseaux et al., 2012; Supekar et al., 2008] and mild cognitive impairment (MCI) [Petrella et al., 2011; Rombouts et al., 2005; Sheline and Raichle, 2013; Sorg et al., 2007]. β -Amyloid and tau deposition in AD and MCI is observed in regions of the default mode network (DMN), such as the precuneus, posterior cingulate cortex, anterior prefrontal cortex, and medial temporal lobe [Arnold et al., 1991]. These brain areas are implicated in self-referential processing, memory, and executive function, and importantly, these brain regions overlap with the areas that show loss of the serotonin transporter (SERT) in MCI [Smith et al., unpublished data].

The serotonin system plays a fundamental role in emotion, cognition, and motivated behaviors [Bell et al., 2001; Canli and Lesch, 2007; Corchs et al., 2015; Cowen and Sherwood, 2013; Schmitt et al., 2006]. While monoamine deficits are consistently reported in post-mortem and neuroimaging studies of AD [Hirao et al., 2015; Palmer and DeKosky, 1993], serotonin degeneration is greater and more widespread than degeneration of other monoaminergic,

and even the cholinergic, systems [Baker and Reynolds, 1989; Cross et al., 1986; Nazarali and Reynolds, 1992; Palmer et al., 1998]. Further, cortical serotonin degeneration has been shown to precede substantial cortical β -amyloid deposition and parallels the course of memory deficits to a greater extent than β -amyloid deposition in mouse models of AD. Neuroimaging studies of the serotonin system in MCI and AD have reported reductions of receptors in cortical (e.g. 5HT_{1A} and 5HT_{2A}) and limbic (5HT_{1A}) regions, including regions of the DMN [Hirao et al., 2015]. More recently, decreased SERT has been observed in cortical (including the precuneus), striatal, and limbic regions, as well as in the dorsal raphe nuclei (DRN; location of the cell bodies of origin for the cortical, subcortical, and limbic projections), in MCI that was more extensive than regional cerebral atrophy or cerebral blood flow deficits [Smith et al., unpublished data]. The decreases in SERT were also correlated with deficits in verbal and visual-spatial memory. These findings indicate that serotonin denervation may occur in MCI prior to AD neuropathology or deficits in cerebral blood flow/metabolism. Integrating neuroimaging studies of monoamine transporters or receptors and brain networks is, therefore, a unique opportunity to understand the functional consequences of neurochemical deficits that may occur before β -amyloid deposition, and may provide important mechanistic information that may have therapeutic implications earlier in the course of the disease.

Functional connectivity deficits in AD have been hypothesized to presage β -amyloid deposition [Jones et al., 2016]. Neurochemical deficits, specifically of the serotonin system, may precede β -amyloid deposition and may contribute to these early connectivity deficits [Liu et al., 2008]. There is evidence for a role of the serotonin system in maintaining the integrity of resting-state networks. 5HT_{1A} receptor signaling predicted activity of the posterior cingulate cortex, which is a key node of the DMN, during resting-state as well as performance of an executive function task [Hahn et al., 2012]. Administration of a 5HT_{1A/2A} receptor agonist led to substantial decreases in resting-state activity and connectivity, specifically in the posterior cingulate [Carhart-Harris et al., 2012, 2016; Muthukumaraswamy et al., 2013] and hippocampus [Carhart-Harris et al., 2014]. Administration of the selective serotonin reuptake inhibitor (SSRI) escitalopram produced widespread decreases in long-range resting-state connectivity of most cortical and subcortical areas [Schaefer et al., 2014]. SERT genetic polymorphisms and manipulation of serotonin levels have also been shown

TABLE I. Demographic characteristics for patients with MCI and elderly controls

	MCI (<i>n</i> = 23)	Elderly controls (<i>n</i> = 21)
Age	69.8 ± 6.7	66.5 ± 7.5
Sex (M/F)	15/8	11/10
Years of education	15.8 ± 3.4	15.3 ± 2.5
Mini-Mental Status Examination	27.7 ± 1.8	28.8 ± 1.4*
Neuropsychiatric Inventory (total score)	5.2 ± 5.3	1.1 ± 2.2**
Total California Verbal Learning Test (CVLT) score (sum of trials 1–5)	40.1 ± 11.3	56.5 ± 9.7***
Brief Visual Memory Test (sum of trials 1–5)	13.4 ± 7.4	20.0 ± 4.6**

Significant between-group differences: **P* < 0.05, ***P* < 0.01, ****P* < 0.001.
MCI, mild cognitive impairment.

to affect network functional connectivity [Kunisato et al., 2011; Rao et al., 2007; Wiggins et al., 2012]. Serotonin degeneration may also have secondary effects on other mechanisms (e.g. nodal stress or trophic failure) that would further impair the function of brain networks [Zhou et al., 2012]. Thus, serotonin function may impact resting-state functional brain connectivity, and degeneration of the serotonin system may be related to deficits in functional connectivity observed in MCI and AD.

To evaluate the impact of SERT on resting-state functional connectivity, SERT values from two regions of interest: the DRN (containing cell bodies of origin of the serotonin projections) and the precuneus (a region of cortical serotonin enervation) were correlated with resting state functional connectivity. Both regions show decreased SERT, as well as AD neuropathology in MCI [Rowe et al., 2007, Smith et al., unpublished data]. The hypotheses were tested that DRN SERT in MCI, but not controls, would be associated with decreased functional connectivity in regions of the medial temporal lobe and default mode network and that precuneus SERT would be correlated with decreased functional connectivity with the precuneus and adjacent medial posterior cortical regions (for example, the posterior cingulate cortex).

METHODS

Participant Screening and Selection

Control participants and participants with MCI were recruited via advertisements in the community. All participants underwent cognitive, psychiatric, and medical evaluation prior to the MRI and positron emission tomography (PET) scans. Evaluations included the mini-mental status examination [Folstein et al., 1976], the clinical dementia rating scale (CDR) [Morris, 1993], the neuropsychiatric inventory (NPI) [Cummings et al., 1994], a structured clinical interview (SCID) [First et al., 1995], and a complete physical examination, including neurological examination and laboratory testing, which included complete blood count, blood chemistry, and toxicology screening. The MCI participants were required to have a CDR global score of 0.5, whereas the controls were required to have a CDR global score of 0 (normal). Participants were excluded from the study who had a history of or

active neurological or Axis I psychiatric disorder including substance abuse, who were not medically stable (i.e. if they had poorly controlled hypertension and/or insulin dependent diabetes), or if they used prescription or over-the-counter medications that affected the central nervous system (e.g. antihistamines, cold medications) in the past 2 weeks prior to enrollment. None of the participants had previously taken an antidepressant. Written informed consent was obtained according to procedures established by the Institutional Review Board and the Radiation Safety Committee of the Johns Hopkins University School of Medicine.

Twenty-three patients with MCI (mean age = 69.8 ± 6.7, 15 males) and 21 healthy controls (mean age = 66.5 ± 7.5, 11 males) were enrolled and underwent both MRI and PET scanning. These participants are a subset of the participants described in a report of the PET results only [Smith et al., unpublished data]. As described below, three MCI participants were excluded due to motion during resting-state scans, yielding a final sample for analysis of 20 patients with MCI and 21 healthy controls. Demographic characteristics for each group are shown in Table I. The groups did not differ significantly in age, sex, or education (*P* > 0.05). All of the MCI participants in the sample underwent β-amyloid imaging ([¹¹C]-PiB; *N*-methyl-[¹¹C]2-(4'-methylaminophenyl)-6-hydroxybenzothiazole) and demonstrated a distribution volume ratio that is associated with cognitive decline (1.2 or higher for anterior [anterior cingulate or middle frontal cortex] and or posterior cortical regions [superior temporal, precuneus, or posterior cingulate; data not shown] [Resnick et al., 2010]). In addition, all of the MCI participants performed at least one standard deviation below the normative value for the California Verbal Learning Test, the Brief Visual Memory Test, or both (data not shown). Thus, this is an MCI sample that is highly likely to demonstrate cognitive decline [Resnick et al., 2010]. One of the controls and two of the MCI participants were left handed.

MRI Acquisition and Preprocessing

MRI data were acquired using a Phillips 3.0T Achieva MRI instrument with an eight-channel head coil (Philips

Medical Systems, Best, Netherlands) at the F. M. Kirby Research Center for Functional Brain Imaging of the Kennedy Krieger Institute. Detailed acquisition parameters for standard imaging sequences and reliability estimates at the F. M. Kirby Research Center are detailed elsewhere [Landman et al., 2011]. A high-resolution structural image (three-dimension magnetization-prepared rapid gradient-echo [MPRAGE]; TE = 4, TR = 8.9, flip angle = 8°, NSA = 1, 0.7 mm slice thickness) was collected for each participant. Resting-state blood-oxygen-level dependent (BOLD) data were also collected for each participant. Participants were scanned in a quiet, darkened room and were instructed to keep their eyes open. BOLD data for each participant consisted of 210 volumes of two-dimensional echo-planar images (EPIs; 3 × 3 mm in-plane resolution, 3 mm slice thickness, 1 mm gap, 37 sequential slices, TR/TE = 2,000/30 ms, flip angle = 75°, with a sensitivity encoding (SENSE) parallel imaging acceleration factor of 2, for a total acquisition time of 7 min).

Each participant's EPI data were slice-timing corrected, realigned to the first acquired volume, and co-registered to the participant's MPRAGE using the normalized mutual information algorithm. The MPRAGE was segmented into gray matter, white matter, and cerebrospinal fluid (CSF) masks, and then normalized to the MNI152 template through indirect normalization, which implements non-linear registration through registration of gray-matter masks to a tissue probability map for the MNI152 template [Ashburner and Friston, 2005]. MPRAGE normalization parameters were propagated to co-registered EPI volumes. EPI data were normalized to the MNI template space and resliced to consist of 2 mm isotropic voxels, and smoothed with a 5mm full width at half maximum (FWHM) kernel. Slice-timing correction and spatial preprocessing steps were completed in Statistical Parametric Mapping version 8 (SPM8; <http://www.fil.ion.ucl.ac.uk/spm>).

An index of head movement, mean relative displacement (MRD), was calculated as in Power [Power et al., 2012] and individuals with gross motion (>0.50 MRD) were excluded [Power et al., 2014]. Three patients with MCI were excluded for gross motion. MRD for the remaining participants did not differ significantly ($M_{\text{controls}} = 0.158$, $M_{\text{MCI}} = 0.182$, $t = 0.751$, $P = 0.457$). Outlier volumes for the remaining participants were scrubbed after preprocessing. Outliers were identified in the ART (https://www.nitrc.org/projects/artifact_detect) toolbox using conservative thresholds (global signal z-value >3, composite measure of total motion across translation and rotation >0.5 mm). A combination of the anatomical CompCor method (aCompCor) [Behzadi et al., 2007] and comprehensive motion artifact regression [Satterthwaite et al., 2013] was used to correct for artifacts in resting-state data related to motion and non-neural physiological artifact. aCompCor improves upon the ability to detect neural signal in the presence of non-neural physiological (e.g. cardiac fluctuations and respiration) and non-physiological (e.g. motion) changes in BOLD signal and

does not require either the measurement of physiological indices (e.g. heart rate or respiration) [Behzadi et al., 2007] or regression of the global signal [Chai et al., 2012]. Comprehensive motion artifact regression [Satterthwaite et al., 2013] has been shown to remove motion-related artifacts that remain after aCompCor correction. Linear effects and their first derivatives, as well as the quadratic of linear effects and derivatives, for the following variables were regressed out of the resting-state data: white matter (the first five components from principle components analysis, or PCA, of the average white matter signal), CSF (the first five components from PCA of the average CSF signal), and the six standard motion parameters (x , y , z translations and rotations). White matter and CSF masks were generated during MPRAGE segmentation, resliced and normalized to the space of preprocessed EPI (2 mm isotropic voxels), and eroded by one voxel. Despiking with a hyperbolic tangent function was performed after nuisance regression, and motion spike regression was performed using a regressor generated for outlier volumes identified by the ART toolbox. Bandpass filtering ($0.008 \geq f \geq 0.09$ Hz) was performed after nuisance regression [Hallquist et al., 2013; Satterthwaite et al., 2013]. Use of the derivative of root mean squared (rms) variance over voxels (DVARs) and voxel-wise displacement parameters have previously been shown to not improve the removal of motion artifact above comprehensive motion parameters and despiking [Satterthwaite et al., 2013]; thus, these parameters were not used here. ROIs were then extracted for statistical analysis. ROIs consisted of 84 unilateral Brodmann Area ROIs (obtained from the Talairach Daemon atlas) [Lancaster et al., 2000], four resting-state DMN ROIs that were previously shown to have strong intersession reliability [Whitfield-Gabrieli and Nieto-Castanon, 2012], and 20 ROIs from the SPM Anatomy Toolbox [Eickhoff et al., 2005] that identify unilateral regions within the amygdala (including unilateral regions for the superficial, laterobasal, and centromedial complexes) and the hippocampus (including CA1-3, the subiculum, the dentate gyrus, the entorhinal cortex, and the hippocampal-amygdaloid transition region) [Amunts et al., 2005], as these cover middle-temporal regions that have been implicated in AD pathology. A total of 108 ROIs were extracted for the analysis. Gray matter and intracranial volumes were also estimated using Freesurfer (<http://surfer.nmr.mgh.harvard.edu/>), for inclusion as analysis covariates.

PET Acquisition and Preprocessing

PET scans were acquired in the Russell H. Morgan Department of Radiology, Johns Hopkins University School of Medicine, using a High Resolution Research Tomograph scanner (HRRT, Siemens Healthcare, Knoxville, TN), which is a cerium-doped lutetium oxyorthosilicate (Lu25i05[Ce] or LSO) based dedicated brain PET scanner with 2 mm FWHM axial resolution. A thermoplastic mask was modeled to each participant's face and used to reduce head motion

TABLE II. Regions of interest where resting-state functional connectivity with the left hippocampus CA2 region is associated with between-group differences in SERT binding in the DRN

Target	Left hemisphere				Right hemisphere			
	β	T	NC r (SE)	MCI r (SE)	β	T	NC r (SE)	MCI r (SE)
Dentate Gyrus					-0.33	-4.10	0.23 (0.03)	0.20 (0.03)
Subiculum	-0.31	-3.84	0.32 (0.03)	0.28 (0.03)	-0.35	-3.77	0.20 (0.03)	0.19 (0.04)
Hippocampus CA3					-0.34	-4.00	0.29 (0.03)	0.30 (0.02)

SERT, serotonin transporter binding; DRN, dorsal raphe nuclei; β , standardized coefficient indicating the difference between MCI and controls in the strength of association between SERT binding in the DRN and resting-state functional connectivity between the target and the left hippocampus CA2 (thresholded using false discovery rate, $P < 0.05$); NC r (SE), average and standard error of functional connectivity (Pearson product moment correlation) with the left hippocampus CA2 ROI in controls; MCI r (SE), average and standard error of functional connectivity (Pearson product moment correlation) with the left hippocampus CA2 ROI in MCI.

during the PET study. The attenuation maps were generated from a 6-min transmission scan that was performed with a [^{137}Cs] point source prior to the emission scans.

The radiotracer [^{11}C]-3-amino-4-(2-dimethylaminomethyl-phenylsulfanyl)-enzonitrile ([^{11}C]-DASB) was synthesized as described in Wilson et al. [2002] and was used to measure SERT. Dynamic scanning began immediately upon a 15 mCi \pm 10% radiotracer injection and lasted for 90 min. The 90-min list mode data were binned into 30 frames (four 15 s, four 30 s, three 1 min, two 2 min, five 4 min, and twelve 5 min frames). The images for [^{11}C]-DASB were reconstructed using the iterative ordered subset expectation maximization (OS-EM) algorithm (with 6 iterations and 16 subsets) with correction for radioactive decay, dead time, attenuation, scatter, and randoms [Rahmim et al., 2005]. The reconstructed image space consisted of cubic voxels, each 1.22 mm in size, and spanning dimensions of 256 mm (left-to-right) by 256 mm (nasion-to-inion) by 207 mm (neck-to-cranium). The final spatial resolution is expected to be less than 2.5 mm FWHM in three directions [Sossi et al., 2005].

Parametric images of distribution volume ratio (DVR) and transport rate constant ratio (R_1) were generated for the [^{11}C]-DASB data by using the simplified reference tissue model (SRTM) and linear regression with a spatial constraint parametric imaging algorithm [Zhou et al., 2003]. The time activity curve from the cerebellar ROI was used for the input function. As described in prior studies and reviewed by Parsey et al. [2006], the cerebellar ROI was carefully delineated to include the cerebellar gray matter and exclude the white matter and vermis in order to minimize the inclusion of SERT in the reference region. DVR images were co-registered to the participant's MPRAGE image with SPM8 using the normalized mutual information algorithm. Co-registered DVR images were then normalized to the MNI152 T1 template using the fast diffeomorphic registration algorithm (DARTEL) [Ashburner, 2007] and smoothed with an isotropic Gaussian kernel (FWHM 3mm). Left and right DRN ROIs were then extracted for use in analysis. The left and right DRN were identified on the

sagittal plane of the DARTEL-normalized MPRAGE MRI scan following the anatomical landmarks described by Kranz [Kranz et al., 2012]. The DRN ROIs were a standard sphere for all subjects of 3 mm in diameter and placed between the superior and inferior colliculus starting medially and extending laterally. The ROIs were visually inspected on all participants' MRI and PET data for proper anatomical localization. Left and right precuneus ROIs were defined using the automated anatomical labeling atlas [Tzourio-Mazoyer et al., 2002]. Representative values from left and right DRN and left and right precuneus ROIs were extracted from the [^{11}C]-DASB DVR images as the average value in all voxels within each ROI. Left and right DRN values from each participant were very highly correlated ($r=0.91$, $P < 0.0001$). Therefore, left and right DRN values were averaged to yield a single DRN SERT binding value for each participant, for use in subsequent analyses. Left and right precuneus SERT values were not very highly correlated ($r=0.46$, $P < 0.01$) and thus were not averaged, and separate analyses were conducted for left and right precuneus SERT.

Statistical Analysis

Resting-state functional connectivity analysis of BOLD data was conducted using the CONN toolbox [Whitfield-Gabrieli and Nieto-Castanon, 2012]. All pair-wise zero-order Pearson correlations were estimated between all 108 ROIs for each participant. Within-participant correlation matrices were transformed using Fisher's r -to- z transformation and submitted to group-level analysis (corrected for multiple comparisons using false discovery rate, $P < 0.05$), where functional connectivity was compared between groups. ROI pairs with an average connectivity that was not significantly different than zero in either group were excluded from further analysis.

Individual differences in functional connectivity were then predicted by (associated with) SERT in the DRN and the precuneus.

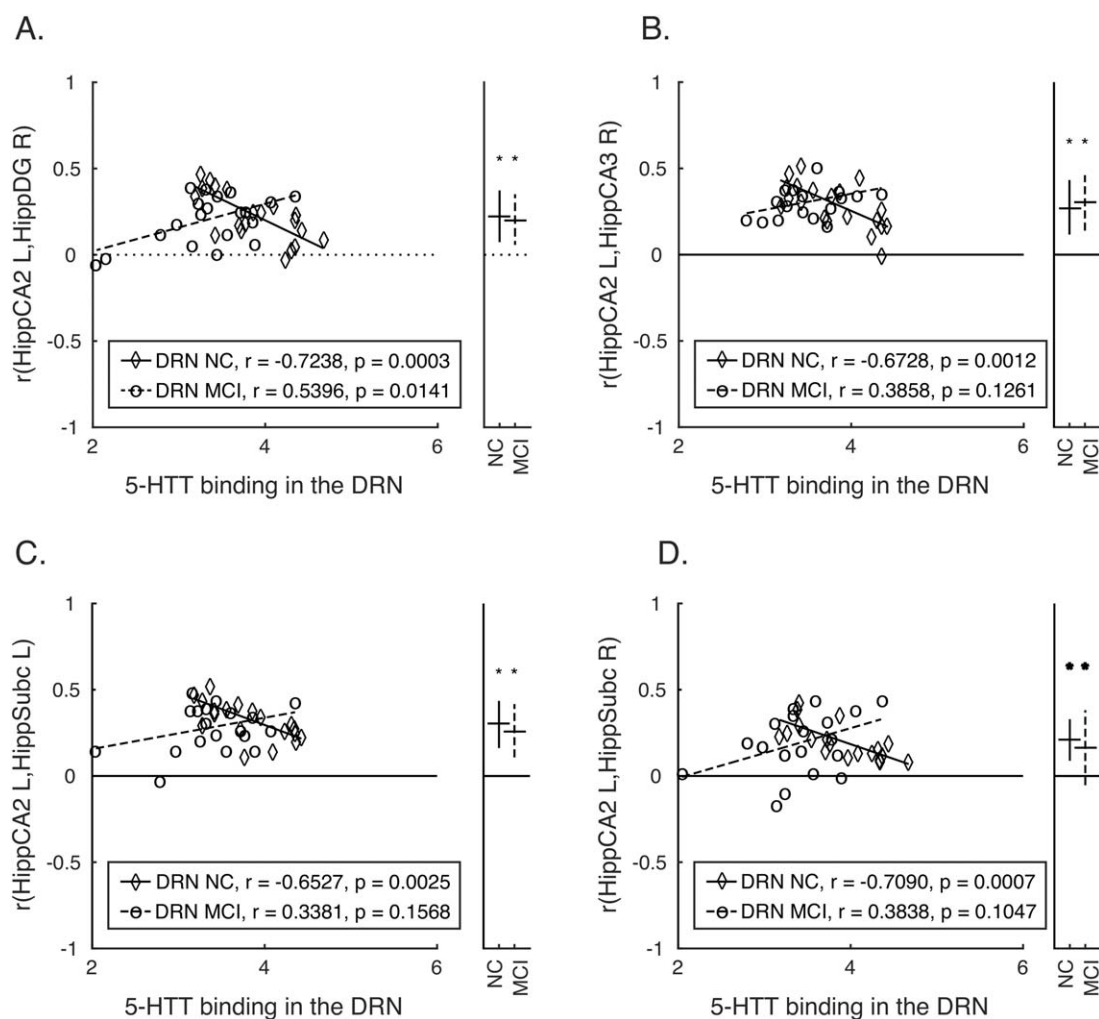


Figure 1.

Group differences in SERT binding in the DRN associated with functional connectivity within hippocampal circuits. (A–D) Correlations between each pair of ROIs (functional connectivity) showing significant between-group differences (depicted in Table II) are plotted against SERT binding values in the DRN for each participant. The ordinate indicates correlation values between two regions (indicated in the y-axis label for each panel), and the abscissa indicates SERT binding values in the DRN. Lines of best fit are plotted separately for each group, and within-group correlations (uncorrected) between functional connectivity

values and SERT binding are listed in the figure legend. The right side of each panel contains an additional axis where the average and standard deviation of the correlation (calculated after Fisher's *r*-to-*z* transformation, and converted back to *r* values for the purpose of plotting) between a given pair of regions indicated in the y-axis label for each group (controls and MCI) is plotted. Average correlations that are significant ($P < 0.05$) are indicated with an asterisk. BA, Brodmann Area; DRN, dorsal raphe nucleus; MCI, mild cognitive impairment; NC, normal control.

The interaction of group and SERT on functional connectivity measures was investigated for each SERT ROI (DRN, left precuneus, right precuneus). Gray matter volume of the left or right precuneus, corrected for total intracranial volume, was also included as a covariate in analyses that included the left or right precuneus SERT measures, respectively. Analyses that included DRN SERT did not include a measure of DRN volume, as the DRN ROI was a fixed size across subjects. Results were corrected for multiple

comparisons between all ROIs (false discovery rate, $P < 0.05$). Post hoc analyses of the relationship between SERT binding and functional connectivity were calculated separately among the controls and MCI cohorts for those pairs of regions that were shown to be significantly different in the interaction analysis for each SERT ROI. Two MCI participants were suspected outliers as they exhibited very low SERT. The possibility that these participants might be exerting high influence on regression results in analyses of the

TABLE III. Between-group differences in SERT binding in the right precuneus associated with resting-state functional connectivity

Target	BA	Seed region							
		Left hemisphere				Right hemisphere			
		β	T	NC r (SE)	MCI r (SE)	β	T	NC r (SE)	MCI r (SE)
Dorsolateral prefrontal cortex	46	-1.90	-3.80	-0.12 (0.04)	-0.12 (0.04)	BA29 (L) Retrosplenial cortex			
Retrosplenial cortex	29					2.03	3.89	0.47 (0.03)	0.51 (0.05)

SERT, Serotonin transporter binding; β , standardized coefficient indicating the difference between MCI and controls in the strength of association between SERT binding in the right precuneus and resting-state functional connectivity between the target and the seed region (thresholded using false discovery rate, $P < 0.05$); NC r (SE), average and standard error of functional connectivity (Pearson product moment correlation) of the target with the seed region in controls; MCI r (SE), average and standard error of functional connectivity (Pearson product moment correlation) of the target with the seed region in MCI.

effect of SERT on individual ROI pairs was evaluated. To protect against such observations that may have unreasonably high influence on model outcomes, Cook's Distance was calculated as a metric of influence, and SERT values for a given participant were excluded from a given analysis of ROI pairs if they yielded a Cook's Distance that was three standard deviations or greater from the mean Cook's Distance for the sample. In most cases, the two participants in question with very low SERT did not exert high influence on regression results. No more than two observations in any given comparison were excluded on the basis of a Cook's Distance value three standard deviations or greater than the mean for the sample, and no participant was excluded from more than four ROI comparisons.

RESULTS

No differences in functional connectivity were observed between controls and patients with MCI. DRN SERT binding values were significantly lower in MCI than in controls ($M_{\text{MCI}} = 3.35$, $SD_{\text{MCI}} = 0.57$; $M_{\text{Control}} = 3.83$, $SD_{\text{Control}} = 0.48$; $t = 4.10$, $P < 0.0005$). Precuneus SERT binding values were significantly lower in MCI than in controls in both the left precuneus ($M_{\text{MCI}} = 1.19$, $SD_{\text{MCI}} = 0.18$; $M_{\text{Control}} = 1.32$, $SD_{\text{Control}} = 0.14$; $t = 2.51$, $P = 0.017$) and right precuneus ($M_{\text{MCI}} = 0.80$, $SD_{\text{MCI}} = 0.09$; $M_{\text{Control}} = 0.95$, $SD_{\text{Control}} = 0.12$; $t = 4.35$, $P < 0.0001$). Gray matter volume did not differ significantly between controls and MCI for the left precuneus ($t = 1.68$, $P = 0.101$) or right precuneus ($t = 1.42$, $P = 0.163$).

Relationship Between Resting-State Functional Connectivity and SERT Binding in the DRN

Decreased SERT in the DRN (Table II) was associated with lower levels of functional connectivity in MCI and higher levels of functional connectivity in controls between the CA2 region of the left hippocampus and the right

dentate gyrus (Fig. 1A). Functional connectivity of the CA2 region of the left hippocampus with the right CA3 region (Fig. 1B) and subicula bilaterally (Fig. 1C,D) was greater with decreased SERT in the DRN in controls, and showed positive, but not significant correlation (i.e. higher levels of connectivity with increased DRN SERT) in MCI.

Relationship Between Resting-State Functional Connectivity and SERT Binding in the Precuneus

Decreased SERT in the right precuneus (Table III) was associated with decreased functional connectivity in MCI and increased functional connectivity in controls between left dorsolateral prefrontal cortex (BA 46) and the left retrosplenial cortex (BA 29; Fig. 2A). Decreased SERT in the right precuneus was associated with increased functional connectivity in MCI, and trended towards positive correlation in controls (i.e. decreased SERT in right precuneus associated with increased functional connectivity) in controls, between the right retrosplenial cortex (BA 29) and the left dorsal posterior cingulate cortex (BA 31; Fig. 2B). The effects of right precuneus gray matter volume covariates for each ROI pair were not significant. No significant associations were observed between SERT in the left precuneus and functional connectivity of any ROI pair.

DISCUSSION

The results of the present study have shown that serotonin denervation (as indexed by decreased SERT) in the DRN is associated with altered functional connectivity of regions of the hippocampal complex (Fig. 1A–D). The hippocampal complex is well-established as a brain region that supports memory formation, consolidation, and retrieval [Carr et al., 2011; Murty et al., 2010]. The hippocampus is also implicated in memory impairment and shows early pathology in MCI and AD [Leal and Yassa,

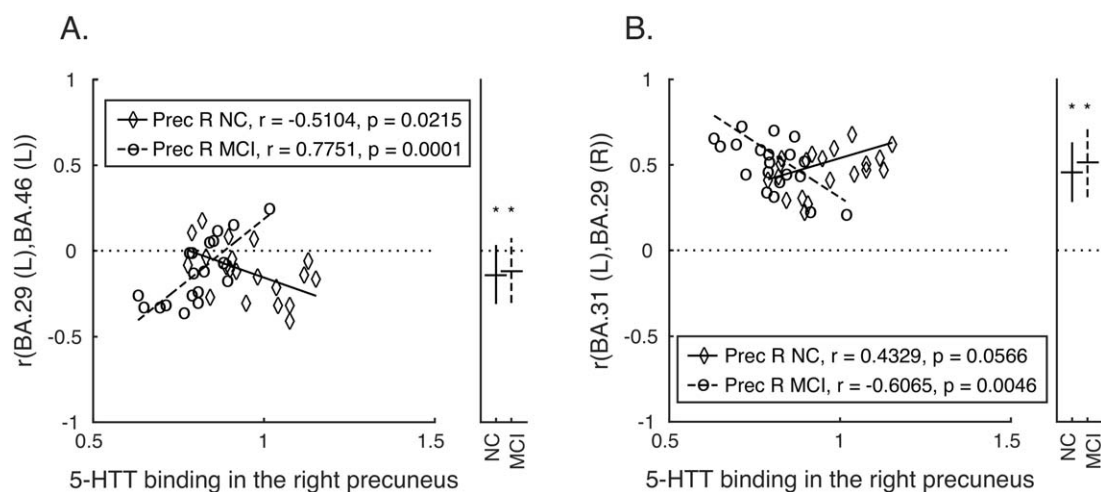


Figure 2.

Group differences in SERT binding in the right precuneus associated with functional connectivity among cortical regions. Correlations between each pair of ROIs (functional connectivity) showing significant between-group differences (depicted in Table III) are plotted against SERT binding values from the right precuneus for each participant. Panels as in Figure 1. BA, Brodmann Area; Prec R, right precuneus; MCI, mild cognitive impairment; NC, normal control.

2013]. Specific serotonergic projections from the DRN to regions of the hippocampus have been previously established [Azmitia and Segal, 1978; Vertes, 1991], and serotonergic projections from the DRN play a critical role in supporting neurogenesis in the hippocampus, which is critical for learning and memory [Alenina and Klempin, 2015]. Deficits in both structural and functional connectivity in this region have been demonstrated in MCI and early AD [Zhang et al., 2009; Zhou et al., 2008]. Thus, the reported findings are consistent with the neurobiology of the hippocampus and the serotonin system, and provide insight into the relationship between central serotonergic functioning (in the DRN) and functional connectivity of brain regions that are implicated in MCI and have been shown to express AD pathology. However, the reported connectivity results must be considered with some caution, since hippocampal subfields are small structures, and the current findings are based on standard fMRI resolution. Future investigations should seek to replicate these findings using high-resolution functional imaging of the medial temporal lobe.

While SERT binding in the DRN was associated with connectivity of regions of the hippocampus, all but one of these effects was found between connectivity of contralateral rather than ipsilateral ROIs. This may suggest serotonergic involvement in signaling across hippocampal commissural projections, which have been demonstrated in the subiculum, dentate gyrus, and regio inferior regions (which roughly correspond to CA2 and CA3 regions of the hippocampus) [Amaral et al., 1984; Gloor et al., 1993].

The present study also demonstrated that higher levels of functional connectivity between the retrosplenial cortex

(which has close proximity to the precuneus) and the dorsal lateral prefrontal cortex (DLPFC) are associated with serotonin denervation in the right precuneus (Fig. 2). Precuneus gray matter volumes were included in the analyses to address potential effects of volumetric differences between subjects. The results remained significant after covarying for precuneus volume; however, no significant associations were observed between left precuneus SERT and brain functional connectivity. Increased connectivity of executive control networks with DMN regions adjacent to the precuneus has previously been reported in AD [Agosta et al., 2012; Damoiseaux et al., 2012] but not in MCI [Agosta et al., 2012]. These results suggest that loss of serotonin innervation may be associated with network dysfunction in MCI.

Several issues should be considered in the interpretation of the findings from this study. If an association between cortical serotonin degeneration and AD pathology were well-established in the literature, SERT in the precuneus might represent a secondary effect of AD pathology, rather than a primary effect of serotonin neurodegeneration. Also, precuneus volumes were included as a covariate to address the possible effects of volumetric changes of the precuneus on the SERT measurements. However, SERT in the DRN could also be affected by partial volume effects. DRN volumes could not be determined because the DRN does not have well-defined boundaries that can be delineated on an MRI scan.

Observing an association between interindividual differences in functional connectivity and SERT raises the question of whether changes in the serotonin system could be an effective target for treatment to modulate network function. Longitudinal evaluation of multimodality imaging of

SERT and resting-state fMRI is supported by the present results with respect to assessing whether the reported associations predict and correlate with subsequent cognitive decline in MCI. As mentioned in the introduction, evidence from animal models suggests that serotonin degeneration may occur early in the course of AD and serotonin agents may have multiple relevant therapeutic mechanisms [Liu et al., 2008; Meneses et al., 2011]. If serotonergic dysfunction in MCI leads to decline of resting-state connectivity and cognitive function, serotonergic agents may improve cognition and potentially slow cognitive decline.

CONCLUSION

While average functional connectivity values did not differ between controls and patients with MCI, individual differences in SERT in the DRN and precuneus predicted individual differences in functional connectivity in patients with MCI. The findings demonstrate an impact of loss of SERT in the DRN and precuneus on subcortical and cortical functional connectivity in patients with MCI and highlight the role of the serotonin system in individual variation in limbic and cortical functional connectivity.

ACKNOWLEDGMENTS

The authors gratefully acknowledge Karen Edmonds, Bineyam Gebrewold, Michael Hans, Jose Leon, and David J. Clough for their invaluable contribution to the acquisition of the PET data; Terri Brawner, Ivana Kusevic, and Kathleen Kahl for their invaluable contribution to the acquisition of the MR data; HRRT technical expertise with reconstruction (Andrew Crabb, MS) and PET scanner quantification (Arman Rahmim, PhD).

REFERENCES

Agcaoglu O, Miller R, Mayer AR, Hugdahl K, Calhoun VD (2015): Lateralization of resting state networks and relationship to age and gender. *Neuroimage* 1;104:310–325.

Agosta F, Pievani M, Geroldi C, Copetti M, Frisoni GB, Filippi M (2012): Resting state fMRI in Alzheimer's disease: beyond the default mode network. *Neurobiol Aging* 33:1564–1578.

Alenina N, Klempin F (2015): The role of serotonin in adult hippocampal neurogenesis. *Behav Brain Res* 277:49–57.

Amaral DG, Insausti R, Cowan WM (1984): The commissural connections of the monkey hippocampal formation. *J Comp Neurol* 224:307–336.

Amunts K, Kedo O, Kindler M, Pieperhoff P, Mohlberg H, Shah NJ, Habel U, Schneider F, Zilles K (2005): Cytoarchitectonic mapping of the human amygdala, hippocampal region and entorhinal cortex: Intersubject variability and probability maps. *Anat Embryol (Berl)* 210:343–352.

Arnold SE, Hyman BT, Flory J, Damasio AR, Van Hoesen GW (1991): The topographical and neuroanatomical distribution of neurofibrillary tangles and neuritic plaques in the cerebral cortex of patients with Alzheimer's disease. *Cereb Cortex* 1:103–116.

Ashburner J (2007): A fast diffeomorphic image registration algorithm. *Neuroimage* 38:95–113.

Ashburner J, Friston KJ (2005): Unified segmentation. *Neuroimage* 26:839–851.

Azmitia EC, Segal M (1978): An autoradiographic analysis of the differential ascending projections of the dorsal and median raphe nuclei in the rat. *J Comp Neurol* 179:641–667.

Baker GB, Reynolds GP (1989): Biogenic amines and their metabolites in Alzheimer's disease: noradrenaline, 5-hydroxytryptamine and 5-hydroxyindole-3-acetic acid depleted in hippocampus but not in substantia innominata. *Neurosci Lett* 100:335–339.

Behzadi Y, Restom K, Liu J, Liu TT (2007): A component based noise correction method (CompCor) for BOLD and perfusion based fMRI. *Neuroimage* 37:90–101.

Bell C, Abrams J, Nutt D (2001): Tryptophan depletion and its implications for psychiatry. *Br J Psychiatry* 178:399–405.

Buckner RL, Andrews-Hanna JR, Schacter DL (2008): The brain's default network: anatomy, function, and relevance to disease. *Ann NY Acad Sci* 1124:1–38.

Canli T, Lesch KP (2007): Long story short: The serotonin transporter in emotion regulation and social cognition. *Nat Neurosci* 10: 1103–1109.

Carhart-Harris RL, Erritzoe D, Williams T, Stone JM, Reed LJ, Colasanti A, Tyacke RJ, Leech R, Malizia AL, Murphy K, Hobden P, Evans J, Feilding A, Wise RG, Nutt DJ (2012): Neural correlates of the psychedelic state as determined by fMRI studies with psilocybin. *Proc Natl Acad Sci USA* 109: 2138–2143.

Carhart-Harris RL, Leech R, Hellyer PJ, Shanahan M, Feilding A, Tagliazucchi E, Chialvo DR, Nutt D (2014): The entropic brain: a theory of conscious states informed by neuroimaging research with psychedelic drugs. *Front Hum Neurosci* 8:20.

Carhart-Harris RL, Muthukumaraswamy S, Roseman L, Kaalen M, Droog W, Murphy K, Tagliazucchi E, Schenberg EE, Nest T, Orban C, Leech R, Williams LT, Williams TM, Bolstridge M, Sessa B, McGonigle J, Sereno MI, Nichols D, Hellyer PJ, Hobden P, Evans J, Singh KD, Wise RG, Curran HV, Feilding A, Nutt DJ (2016): Neural correlates of the LSD experience revealed by multimodal neuroimaging. *Proc Natl Acad Sci USA* 113:4853–4858.

Carr MF, Jadhav SP, Frank LM (2011): Hippocampal replay in the awake state: A potential substrate for memory consolidation and retrieval. *Nat Neurosci* 14:147–153.

Chai XJ, Castanon AN, Ongur D, Whitfield-Gabrieli S (2012): Anticorrelations in resting state networks without global signal regression. *Neuroimage* 59:1420–1428.

Corchs F, Nutt DJ, Hince DA, Davies SJ, Bernik M, Hood SD (2015): Evidence for serotonin function as a neurochemical difference between fear and anxiety disorders in humans? *J Psychopharmacol* 29:1061–1069.

Cowen P, Sherwood AC (2013): The role of serotonin in cognitive function: evidence from recent studies and implications for understanding depression. *J Psychopharmacol* 27:575–583.

Cross AJ, Crow TJ, Ferrier IN, Johnson JA (1986): The selectivity of the reduction of serotonin S2 receptors in Alzheimer-type dementia. *Neurobiol Aging* 7:3–7.

Cummings JL, Mega M, Gray K, Rosenberg-Thompson S, Carusi DA, Gornbein J (1994): The Neuropsychiatric Inventory: Comprehensive assessment of psychopathology in dementia. *Neurology* 44:2308–2314.

Damoiseaux JS, Beckmann CF, Arigita EJ, Barkhof F, Scheltens P, Stam CJ, Smith SM, Rombouts SARB (2008): Reduced resting-

- state brain activity in the “default network” in normal aging. *Cereb Cortex* 18:1856–1864.
- Damoiseaux JS, Greicius MD (2009): Greater than the sum of its parts: a review of studies combining structural connectivity and resting-state functional connectivity. *Brain Struct Funct* 213:525–533.
- Damoiseaux JS, Prater KE, Miller BL, Greicius MD (2012): Functional connectivity tracks clinical deterioration in Alzheimer’s disease. *Neurobiol Aging* 33:828.e30. Apr
- Damoiseaux JS, Rombouts SA, Barkhof F, Scheltens P, Stam CJ, Smith SM, Beckmann CF (2006): Consistent resting-state networks across healthy subjects. *Proc Natl Acad Sci USA* 103:13848–13853.
- Eickhoff SB, Stephan KE, Mohlberg H, Grefkes C, Fink GR, Amunts K, Zilles K (2005): A new SPM toolbox for combining probabilistic cytoarchitectonic maps and functional imaging data. *Neuroimage* 25:1325–1335.
- Ferreira LK, Busatto GF (2013): Resting-state functional connectivity in normal brain aging. *Neurosci Biobehav Rev* 37:384–400.
- First M, Spitzer R, Gibbon M, Williams J (1995): Structured Clinical Interview for DSM-IV Axis 1 Disorders-Patient Edition (SCID-I/P). New York: New York Psychiatric Institute.
- Folstein M, Folstein S, McHugh P (1976): Mini-mental state. *J Psychiatric Res* 12:198.
- Fox MD, Raichle ME (2007): Spontaneous fluctuations in brain activity observed with functional magnetic resonance imaging. *Nat Rev Neurosci* 8:700–711.
- Gloor P, Salanova V, Olivier A, Quesney LF (1993): The human dorsal hippocampal commissure. An anatomically identifiable and functional pathway. *Brain* 116:1249–1273.
- Greicius MD, Supekar K, Menon V, Dougherty RF (2009): Resting-state functional connectivity reflects structural connectivity in the default mode network. *Cereb Cortex* 19:72–78.
- Hahn A, Wadsak W, Windischberger C, Baldinger P, Hoflich AS, Losak J, Nics L, Philippe C, Kranz GS, Kraus C, Mitterhauser M, Karanikas G, Kasper S, Lanzemberger R (2012): Differential modulation of the default mode network via serotonin-1A receptors. *Proc Natl Acad Sci USA* 109:2619–2624.
- Hallquist MN, Hwang K, Luna B (2013): The nuisance of nuisance regression: Spectral misspecification in a common approach to resting-state fMRI preprocessing reintroduces noise and obscures functional connectivity. *Neuroimage* 82:208–225.
- Hirao K, Pontone GM, Smith GS (2015): Molecular imaging of neuropsychiatric symptoms in Alzheimer’s and Parkinson’s disease. *Neurosci Biobehav Rev* 49:157–170.
- Jones DT, Knopman DS, Gunter JL, Graff-Radford J, Vemuri P, Boeve BF, Petersen RC, Weiner MW, Jack CR (2016): Cascading network failure across the Alzheimer’s disease spectrum. *Brain* 139:547–562.
- Keller JB, Hedden T, Thompson TW, Anteraper SA, Gabrieli JD, Whitfield-Gabrieli S (2015): Resting-state anticorrelations between medial and lateral prefrontal cortex: association with working memory, aging, and individual differences. *Cortex* 64:271–280.
- Kranz GS, Hahn A, Savli M, Lanzemberger R (2012): Challenges in the differentiation of midbrain raphe nuclei in neuroimaging research. *Proc Natl Acad Sci USA* 109:E2000.
- Kunisato Y, Okamoto Y, Okada G, Aoyama S, Demoto Y, Munakata A, Nomura M, Onoda K, Yamawaki S (2011): Modulation of default-mode network activity by acute tryptophan depletion is associated with mood change: A resting state functional magnetic resonance imaging study. *Neurosci Res* 69:129–134.
- Lancaster JL, Woldorff MG, Parsons LM, Liotti M, Freitas CS, Rainey L, Kochunov PV, Nickerson D, Mikiten SA, Fox PT (2000): Automated Talairach atlas labels for functional brain mapping. *Hum Brain Mapp* 10:120–131.
- Landman BA, Huang AJ, Gifford A, Vikram DS, Lim IA, Farrell JA, Bogovic JA, Hua J, Chen M, Jarso S, Smith SA, Joel S, Mori S, Pekar JJ, Barker PB, Prince JL, van Zijl PC (2011): Multi-parametric neuroimaging reproducibility: a 3-T resource study. *Neuroimage* 54:2854.
- Leal SL, Yassa MA (2013): Perturbations of neural circuitry in aging, mild cognitive impairment, and Alzheimer’s disease. *Ageing Res Rev* 12:823–831.
- Liu Y, Yoo MJ, Savonenko A, Stirling W, Price DL, Borchelt DR, Mamounas L, Lyons WE, Blue ME, Lee MK (2008): Amyloid pathology is associated with progressive monoaminergic neurodegeneration in a transgenic mouse model of Alzheimer’s disease. *J Neurosci* 28:13805–138014.
- Meneses A, Perez-Garcia G, Ponce-Lopez T, Tellez R, Castillo C (2011): Serotonin transporter and memory. *Neuropharmacology* 61:355–363.
- Morris JC (1993): The Clinical Dementia Rating (CDR): Current version and scoring rules. *Neurology* 43:2412–2414.
- Murty VP, Ritchey M, Adcock RA, LaBar KS (2010): fMRI studies of successful emotional memory encoding: A quantitative meta-analysis. *Neuropsychologia* 48:3459–3469.
- Muthukumaraswamy SD, Carhart-Harris RL, Moran RJ, Brookes MJ, Williams TM, Errizoe D, Sessa B, Padapopoulos A, Bolstridge M, Singh KD, Feilding A, Friston KJ, Nutt DJ (2013): Broadband cortical desynchronization underlies the human psychedelic state. *J Neurosci* 33:15171–15118.
- Nazarali AJ, Reynolds GP (1992): Monoamine neurotransmitters and their metabolites in brain regions in Alzheimer’s disease: A postmortem study. *Cell Mol Neurobiol* 12:581–587.
- Palmer AM, DeKosky ST (1993): Monoamine neurons in aging and Alzheimer’s disease. *J Neural Transm Gen Sect* 91:135–159.
- Palmer AM, Stratmann GC, Procter AW, Bowen DM (1988): Possible neurotransmitter basis of behavioral changes in Alzheimer’s disease. *Ann Neurol* 23:616–620.
- Parsey RV, Kent JM, Oquendo MA, Richards MC, Pratap M, Cooper TB, Arango V, Mann JJ (2006): Acute occupancy of brain serotonin transporter by sertraline as measured by [¹¹C]DASB and positron emission tomography. *Biol Psychiatry* 59:821–828.
- Petrella JR, Sheldon FC, Prince SE, Calhoun VD, Doraiswamy PM (2011): Default mode network connectivity in stable vs progressive mild cognitive impairment. *Neurology* 76:511–517.
- Power JD, Barnes KA, Snyder AZ, Schlaggar BL, Petersen SE (2012): Spurious but systematic correlations in functional connectivity MRI networks arise from subject motion. *Neuroimage* 59:2142–2154.
- Power JD, Mitra A, Laumann TO, Snyder AZ, Schlaggar BL, Petersen SE (2014): Methods to detect, characterize, and remove motion artifact in resting state fMRI. *Neuroimage* 84:320–341.
- Rahmim A, Cheng JC, Blinder S, Camborde ML, Sossi V (2005): Statistical dynamic image reconstruction in state-of-the-art high-resolution PET. *Phys Med Biol* 50:4887–4912.
- Rao H, Gillihan SJ, Wang J, Korczykowski M, Sankoorikal GM, Kaercher KA, Brodtkin ES, Detre JA, Farah MJ (2007): Genetic variation in serotonin transporter alters resting brain function in healthy individuals. *Biol Psychiatry* 62:600–606.
- Resnick SM, Sojkova J, Zhou Y, An Y, Ye W, Holt DP, Dannals RF, Mathis CA, Klunk WE, Ferrucci L, Kraut MA, Wong DF

- (2010): Longitudinal cognitive decline is associated with fibrillar amyloid-beta measured by [11C]PiB. *Neurology* 74:807–815.
- Rombouts SA, Barkhof F, Goekoop R, Stam CJ, Scheltens P (2005): Altered resting state networks in mild cognitive impairment and mild Alzheimer's disease: An fMRI study. *Hum Brain Mapp* 26:231–239.
- Rowe CC, Ng S, Ackermann U, Gong SJ, Pike K, Savage G, Cowie TF, Dickinson KL, Maruff P, Darby D, Smith C, Woodward M, Merory J, Tochon-Danguy H, O'Keefe G, Klunk WE, Mathis CA, Price JC, Masters CL, Villemagne VL (2007): Imaging beta-amyloid burden in aging and dementia. *Neurol* 68:1718–1725.
- Satterthwaite TD, Elliott MA, Gerraty RT, Ruparel K, Loughhead J, Calkins ME, Eickhoff SB, Hakonarson H, Gur RC, Gur RE, Wolf DH (2013): An improved framework for confound regression and filtering for control of motion artifact in the preprocessing of resting-state functional connectivity data. *Neuroimage* 64:240–256.
- Schaefer A, Burmann I, Regenthal R, Arelin K, Barth C, Pampel A, Villringer A, Margulies DS, Sacher J (2014): Serotonergic modulation of intrinsic functional connectivity. *Curr Biol* 24:2314–2318.
- Schmitt JA, Wingen M, Ramaekers JG, Evers EA, Riedel WJ (2006): Serotonin and human cognitive performance. *Curr Pharm Des* 12:2473–2486.
- Sheline YI, Raichle ME (2013): Resting state functional connectivity in preclinical Alzheimer's disease. *Biol Psychiatry* 74:340–347.
- Sorg C, Riedl V, Muhlau M, Calhoun VD, Eichele T, Laer L, Drzezga A, Forstl H, Kurz A, Zimmer C, Wohlschlagel AM (2007): Selective changes of resting-state networks in individuals at risk for Alzheimer's disease. *Proc Natl Acad Sci USA* 104:18760–18765.
- Sossi V, De Jong M, Barker W, Bloomfield P, Burbar Z, Welsh RC, Martin DM, Monk CS (2005): The second generation HRRT: A multi-centre scanner performance investigation. *IEEE Nucl Sci Symp Conf.* 104:18760–18765.
- Smith SM, Fox PT, Miller KL, Glahn DC, Fox PM, Mackay CE, Filippini N, Watkins KE, Toro R, Laird AR, Beckmann CF (2009): Correspondence of the brain's functional architecture during activation and rest. *Proc Natl Acad Sci USA* 106:13040–13045.
- Supekar K, Menon V, Rubin D, Musen M, Greicius MD (2008): Network analysis of intrinsic functional brain connectivity in Alzheimer's disease. *PLoS Comput Biol* 4:e1000100.
- Tzourio-Mazoyer N, Landeau B, Papathanassiou D, Crivello F, Etard O, Delcroix N, Mazoyer B, Joliot M (2002): Automated anatomical labeling of activations in SPM using a macroscopic anatomical parcellation of the MNI MRI single-subject brain. *Neuroimage* 15:273–289.
- van den Heuvel MP, Mandl RC, Kahn RS, Hulshoff Pol HE (2009): Functionally linked resting-state networks reflect the underlying structural connectivity architecture of the human brain. *Hum Brain Mapp* 30:3127–3141.
- van den Heuvel MP, Sporns O (2013): Network hubs in the human brain. *Trends Cogn Sci* 17:683–696.
- Vertes RP (1991): A PHA-L analysis of ascending projections of the dorsal raphe nucleus in the rat. *J Comp Neurol* 313:643–668.
- Whitfield-Gabrieli S, Nieto-Castanon A (2012): Conn: A functional connectivity toolbox for correlated and anticorrelated brain networks. *Brain Connect* 2:125–141.
- Wiggins JL, Bedoyan JK, Peltier SJ, Ashinoff S, Carrasco M, Weng SJ, Welsh RC, Martin DM, Monk CS (2012): The impact of serotonin transporter (5-HTTLPR) genotype on the development of resting-state functional connectivity in children and adolescents: A preliminary report. *Neuroimage* 59:2760–2770.
- Wilson AA, Ginovart N, Hussey D, Meyer J, Houle S (2002): In vitro and in vivo characterisation of [11C]-DASB: a probe for in vivo measurements of the serotonin transporter by positron emission tomography. *Nucl Med Biol* 29:509–515.
- Zhang HY, Wang SJ, Xing J, Liu B, Ma ZL, Yang M, Zhang ZJ, Teng GJ (2009): Detection of PCC functional connectivity characteristics in resting-state fMRI in mild Alzheimer's disease. *Behav Brain Res* 197:103–108.
- Zhou Y, Dougherty JH, Jr, Hubner KF, Bai B, Cannon RL, Hutson RK (2008): Abnormal connectivity in the posterior cingulate and hippocampus in early Alzheimer's disease and mild cognitive impairment. *Alzheimers Dement* 4:265–270.
- Zhou J, Gennatas ED, Kramer JH, Miller BL, Seeley WW (2012): Predicting regional neurodegeneration from the healthy brain functional connectome. *Neuron* 73:1216–1222.
- Zhou Y, Endres CJ, Brasic JR, Huang SC, Wong DF (2003): Linear regression with spatial constraint to generate parametric images of ligand-receptor dynamic PET studies with a simplified reference tissue model. *Neuroimage* 18:975–989.